Nanoscale

ROYAL SOCIETY OF CHEMISTRY

PAPER

View Article Online
View Journal | View Issue

Cite this: *Nanoscale*, 2021, **13**, 2914

Single-particle fibrinogen detection using platelet membrane-coated fluorescent polystyrene nanoparticles†

Da Chen, [a,b] Ziyi Song,[a,c] Meiling Lian,[b] Yi Yang,[c] Shen Lin[c] and Lehui Xiao *[c]

Received 30th November 2020,
Accepted 2nd January 2021

DOI: 10.1039/d0nr08492a

rsc.li/nanoscale

Fibrinogen participates in many physiological processes and is a biomarker for a variety of diseases. On this account, the development of a sensitive method for fibrinogen assay is particularly important. Herein, we demonstrate a new color-coded single-particle detection (SPD) method for fibrinogen detection by using platelet membrane-coated fluorescent polystyrene nanoparticles (PNPs) as the probes. Due to the specific interactions between fibrinogen and integrin receptors on platelet membranes, PNPs can form aggregated structures in the presence of fibrinogen. Therefore, colocalization events between green and red PNPs and the corresponding Pearson's correlation coefficient vary with the concentrations of fibrinogen. The sensing ability shows a linear range of 30–300 μg mL^{-1} and a limit of detection (LOD) of 3.9 μg mL^{-1} (11.3 nM) for fibrinogen detection. Moreover, it has been validated that the proposed biosensor can selectively detect fibrinogen and shows a good performance in real sample applications.

Introduction

Fibrinogen is a 340 kDa plasmatic glycoprotein produced by the liver and participates in the final step of blood coagulation. It plays an important role in capillary formation, angiogenesis, cell differentiation and wound healing.[1,2] The normal fibrinogen concentration range in the human body is 2–4 mg mL^{-1}. It has been reported that abnormal concentrations of fibrinogen in plasma are associated with many diseases. Elevated fibrinogen levels are important biomarkers of cardiovascular diseases,[3] while lower levels indicate the risk of bleeding and are also closely related to liver diseases. Recently, extensive research has shown that fibrinogen is a biomarker of myocardial infarction, atherosclerosis[4] and Alzheimer's disease.[5] In addition, it is also a prognostic blood marker for survival in patients with certain types of cancer.[6–8] Therefore, the development of a sensitive and reliable method for the quantification of fibrinogen is of great significance.

To date, many detection methods have been developed for fibrinogen analysis. For example, the Clauss assay and prothrombin time (PT)-derived assay are commonly used in clinical analysis.[9] However, the outcomes usually depend on the source of commercial reagents, analyzers and experimental conditions.[10] Some physical–chemical methods such as salting-out and heating-precipitation are rapid and simple, but they suffer from low sensitivity and poor selectivity. Some immunological methods can overcome these shortcomings,[11–13] however, they normally require tedious modification procedures and expensive labels. To address these problems, new fibrinogen quantification methods are in urgent demand.

Recently, fibrinogen detection using a cell membrane coating strategy has been developed. In order to detect fibrinogen sensitively, Park *et al.* devised an erythrocyte membrane-blanketed biosensor based on localized surface plasmon resonance.[14] Afterwards, an electrochemical impedance biosensor modified using an erythrocyte membrane was developed.[15] Nowadays, cell membrane-coated nanoparticles are becoming more and more popular in many areas.[16–23] This class of nanomaterials are characterized by nanoparticulate cores coated with membrane derived from various cells, such as red blood cells, white blood cells, platelets, cancer cells or bacteria. The resulting cell membrane-coated nanoparticles can directly replicate the surface properties of source cells such as long circulation time and disease-relevant targeting.[24] Compared with artificial nanomaterials, these biomimetic nanoparticles possess improved anti-interference capability, colloidal stabi-

[a]*School of Precision Instruments and Optoelectronics Engineering, Tianjin University, Tianjin, 300072, China*
[b]*Key Laboratory of Civil Aviation Thermal Hazards Prevention and Emergency Response, Civil Aviation University of China, Tianjin, 300300, China*
[c]*State Key Laboratory of Medicinal Chemical Biology, Tianjin Key Laboratory of Biosensing and Molecular Recognition, College of Chemistry, Nankai University, Tianjin, 300071, China. E-mail: lehuixiao@nankai.edu.cn*

†Electronic supplementary information (ESI) available: Fluorescence colocalization analysis, image processing and analysis, supporting figures and references are described in the manuscript. See DOI: 10.1039/d0nr08492a

lity and targeting specificity. Meanwhile, the immune rejection, toxic effects and adverse reactions associated with unmodified nanoparticles were reduced in biological applications.[25,26] By mimicking the physical properties and complex functions of different cells, cell membrane-coated nanoparticles can identify the corresponding natural ligands. For example, integrins $\alpha_{IIb}\beta_3$ on platelet membranes are known to be specific receptors for fibrinogen.[27] Inspired by this, it will be a promising approach to detect fibrinogen using platelet membrane-coated nanoparticles (PNPs). With the help of the unique characteristics of platelets, PNPs have shown superior performance in various fields.[28,29] However, they have never been used for protein detection. On this account, we have invested our efforts in developing a new fibrinogen quantification method based on PNPs.

In recent years, single-particle detection (SPD) based on optical microscopy imaging has been widely applied in the determination of DNAs, ions, enzymes, proteins, mycotoxins and so on.[30–36] Compared with conventional methods, targets can be quantified with high sensitivity and ultra-low sample consumptions. Inspired by these merits and the advantages of cell membrane-coated nanoparticles mentioned above, our study aims to combine SPD with cell membrane coating technology for the first time. This combination will provide not only high sensitivity and extremely low sample consumption attributed to the single-particle imaging but also excellent selectivity and anti-interference ability in real sample applications due to the coverage of cell membrane.

Herein, a convenient and low-cost fibrinogen quantification method was developed based on SPD and PNPs. In this study, platelet vesicles were wrapped on the surface of green and red fluorescent polystyrene nanoparticles (PS cores) as the probes. The principle of our design is based on the fact that integrins $\alpha_{IIb}\beta_3$ on the surface of the platelet membrane are the specific receptor for fibrinogen. From previous explorations, the single-molecule interaction between fibrinogen and $\alpha_{IIb}\beta_3$ has an average binding force of 97 pN obtained by force spectroscopy measurements.[27] As a consequence, the PNPs will interact with target fibrinogen specifically and form irreversible aggregated structures. As illustrated in Scheme 1, when the green and red PNPs combine with the same target, colocalization of green and red fluorescence spots can be detected which are observed as yellow spots in the merged fluorescence image. However, in the absence of fibrinogen, the particles in the green and red fluorescence channels are well dispersed without any overlap. In addition, the number of colocalization events varies with the concentration of fibrinogen. The experimental results show that the Pearson's correlation coefficient has a linear relationship with the fibrinogen concentration from 30 to 300 μg mL^{-1}. The limit of detection (LOD) is 3.9 μg mL^{-1} (11.3 nM) based on a signal-to-noise ratio of 3. Furthermore, satisfactory recoveries (in the range of 98.3%–105.5%) are obtained in plasma samples which illustrate the promising practical applicability of this method.

Experimental section

Materials and reagents

Fresh bovine whole blood and plasma were purchased from Hongquan Biotechnology Co., Ltd (Guangzhou, China). Green (loaded with Alexa Fluor 488) and red (loaded with Alexa Fluor 633) fluorescent carboxyl polystyrene nanoparticles with a size of 200 nm were purchased from Baseline ChromTech Research Center (Tianjin, China). Fibrinogen (from bovine plasma) was purchased from Meilun Biotechnology Co., Ltd (Dalian, China). Collagen I was purchased from Yuanye Biotechnology Co., Ltd (Shanghai, China). Transferrin human (TF) and thrombin were purchased from Sigma Aldrich (MO, United States). Bovine serum albumin (BSA), immunoglobulin G (IgG) and adenosine 5′-diphosphate sodium salt (ADP) were purchased from Aladdin Reagent Co., Ltd (Shanghai, China). L-Tyrosine (L-Tyr), L-phenylalanine (L-Phe), L-lysine (L-Lys), L-histidine (L-His), glutathione (GSH), sodium chloride (NaCl), potassium chloride (KCl), disodium hydrogen phosphate (Na_2HPO_4), potassium dihydrogen phosphate (KH_2PO_4), magnesium chloride ($MgCl_2{\cdot}6H_2O$) and calcium chloride ($CaCl_2$) were purchased from Sinopharm Chemical Reagent Co., Ltd (Shanghai, China). A polycarbonate membrane (400 nm and 200 nm pore size) and support membrane were purchased from Avanti Polar Lipids (Alabaster, Alabama, USA). 10 mM phosphate buffered saline (PBS) solution with calcium and magnesium (138 mM NaCl, 2.67 mM KCl, 8.1 mM Na_2HPO_4, 1.47 mM KH_2PO_4, 1 mM $CaCl_2$ and 0.5 mM $MgCl_2{\cdot}6H_2O$, pH 7.4) was self-prepared. All of the other chemical reagents used in this work were of analytical grade and all aqueous solutions were prepared with ultra-pure water.

Apparatus

The dynamic light scattering (DLS) data were measured with a Zetasizer Nano ZS System (Malvern, UK) to determine the average diameter and surface charge of samples. The fluorescence spectra of PS cores were recorded with a fluorescence spectrophotometer (F-4600, Hitachi, Japan). The morphological changes of PS cores after wrapping with platelet vesicles were characterized by scanning transmission electron microscopy (STEM, Shimadzu SS-550, Japan). The formation of aggregated structures was verified by scanning electron microscopy (SEM, Shimadzu SS-550, Japan). All fluorescence images were obtained using laser confocal scanning microscopy (LCSM, A1R+, Nikon, Japan) with a 60× objective. 473 and 633 nm lasers were used as excitation sources for green and red PS cores, respectively. Fluorescence images of the green channel (Emission filter: 515–550 nm), red channel (Emission filter: 653–738 nm) and merged channel were acquired with a resolution of 512 × 512 pixels. All images were processed with ImageJ and MATLAB. Briefly, the images were processed by Gaussian blur (σ = 0.6), smoothing and contrast enhancement using ImageJ. The extraction of overlapped points between green and red channels and the drawing of scatter plots were all completed by MATLAB programs (see the ESI†).

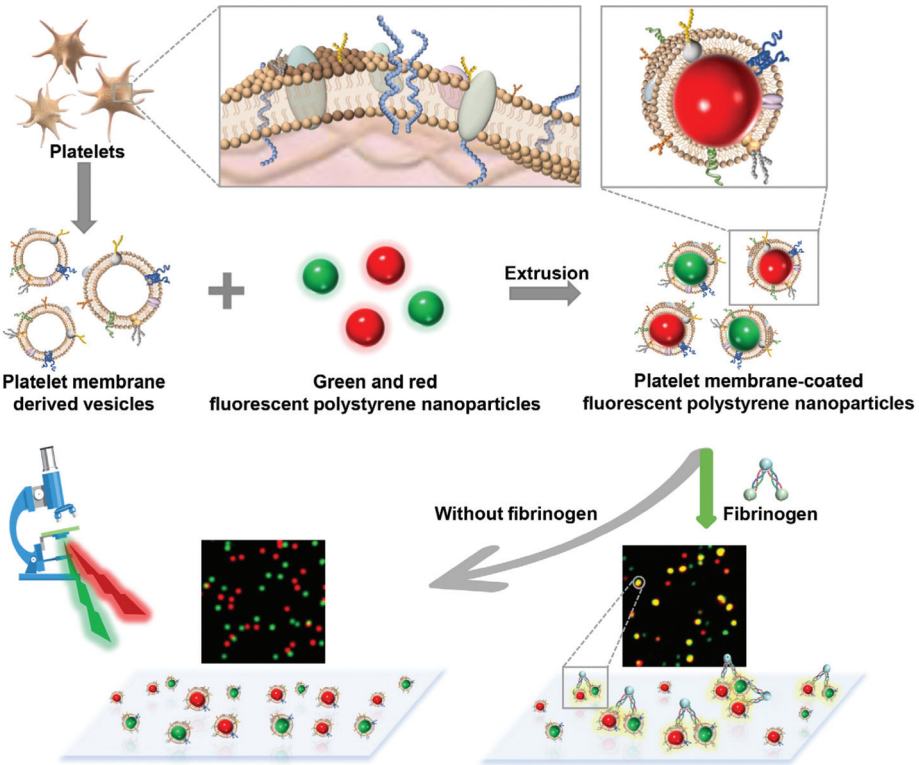

Scheme 1 The scheme of fibrinogen detection using platelet membrane-coated fluorescent polystyrene nanoparticles (PNPs).

Platelet isolation and membrane derivation

Platelets were isolated from whole bovine blood by a previously reported method.[37] Briefly, the blood samples were centrifuged at 300*g* for 5 min first. In order to separate red blood cells and white blood cells completely, the supernatants were collected and spun at the same speed for another 5 min. The resulting supernatants represented platelet rich plasma (PRP). Afterwards, ADP was added to PRP to reach a final concentration of 20 μM. Then, the solutions were centrifuged at 2000*g* for 4 min in order to pellet down the platelets. Finally, the platelets were resuspended in ultra-pure water and stored at −80 °C for further use. The platelet membrane was derived by a repeated freeze–thaw process. A frozen aliquot of platelet solution was thawed at room temperature and centrifuged at 21 000*g* for 5 min. Afterwards, the pellet was resuspended in ultra-pure water and refrozen. The whole process was repeated 3 times. Finally, the pellet which was extracted from 3 mL of whole blood was resuspended in 50 μL of ultra-pure water and sonicated for 5 min at a frequency of 40 kHz. The platelet membrane was obtained ultimately.

Preparation and characterization of PNPs

The membrane was wrapped on the PS cores by a previously reported method.[38] The platelet membrane solution was homogenized with a syringe and physically extruded through a polycarbonate membrane (200 nm pore size) 5 times using a liposome extruder to obtain the platelet vesicles. Afterwards, 50 μL of platelet vesicles and PS cores (20 μg mL^{-1}, 35 μL) were mixed and co-extruded through a polycarbonate membrane (200 nm pore size) 11 times to obtain the PNPs. The size distribution and surface charge of platelets, platelet vesicles, PS cores and PNPs were measured using a Zetasizer Nano ZS system. To verify the morphology of PNPs, samples were deposited onto a copper grid and measured using TEM.

Determination of fibrinogen

Fibrinogen was dissolved in preheated 0.9% NaCl aqueous solution for an hour in a 37 °C water bath (upside down to help it dissolve, without shaking vigorously) and centrifuged to remove the insoluble floccules to obtain the desired fibrinogen solution. For the assay of fibrinogen, 15 μL of green PNPs and 15 μL of red PNPs were added into a series of 200 μL tubes. Subsequently, 30 μL of fibrinogen solutions with different concentrations were added respectively. The solutions were diluted to a final volume of 100 μL with PBS and incubated for 2 hours at 37 °C. Before microscopic imaging, vacuum grease was used to make flow channels on the surface of the amino-modified glass slide. In the SPD detection experiment, 10 μL of reaction samples were injected into a flow channel. The negatively charged PNPs were immobilized on the surface of the amino-modified glass slide through electrostatic interactions. After adsorption of 5 min, fluorescence images were acquired using a LCSM. To investigate the potential applicability of this method, the recovery assay was per-

formed with bovine plasma samples by the standard addition method. Different concentrations of fibrinogen standard solutions (60, 150 and 300 μg mL^{-1}) were added to 1% PBS diluted plasma and analyzed using the procedures described above.

Results and discussion

Fabrication and characterization of PS cores and PNPs

In this work, PNPs are used as the probes for the fibrinogen assay. In order to explore whether the properties of these PS cores are suitable for the subsequent detection, the particles were characterized with spectroscopy and microscopy measurements. First of all, the morphology of PS cores was characterized by SEM. As shown in Fig. S1,† the particles exhibit an excellent spherical morphology and are uniform in size. The fluorescence spectra in Fig. 1a indicate that the excitation wavelengths of green and red PS cores are 475 and 611 nm, and the corresponding emission peaks locate at 499 and 631 nm, respectively. Meanwhile, under the corresponding excitation wavelengths, the PS cores show uniform and bright fluorescence intensity in the LCSM images (Fig. 1b and c), which is suitable for SPD assays. To prepare PNPs, we isolated platelets and their membranes using differential centrifugation and repeated freeze–thaw, respectively. Subsequently, PNPs were prepared by fusing platelet vesicles onto the surface of PS cores. To be specific, platelet vesicles and PS cores (20 μg mL^{-1}) were co-extruded by a liposome extruder. As the degree of encapsulation will affect the detection performance, the coating condition is optimized and characterized by dark-field microscopic imaging. As shown in Fig. S2a,† when the volume ratio of vesicle and PS core was 2 : 1, there were many redundant vesicles which appeared as extremely weak scattering spots. In contrast, slightly increasing the number of particles in the mixture until the volume ratio reached 10 : 7, uniform scattering spots with suitable density could be observed (Fig. S2b†).

After the membrane coating process, the variation of diameter and surface charge of PNPs were measured with DLS. As shown in Fig. 1d, the average diameter of PNPs has an approximately 14 nm increment comparing to the bare PS cores. Subsequently, the zeta potential of PNPs was measured to verify the coverage of the membrane. As shown in Fig. 1e, the core materials show a strong negative charge (−71.45 mV) before the coating process, which is attributed to the carboxyl groups on the surface of PS cores. However, the surface charge of PNPs is almost the same as that of platelet vesicles (approaching the value of −25 mV). This noticeable change indicates that the PS cores have been well covered by a thin layer of platelet membrane. As a more direct evidence, the TEM image of PNPs reveals a characteristic core–shell structure after the membrane coating process (Fig. 1f). Taken together, these results indicate that the PNPs have been prepared successfully.

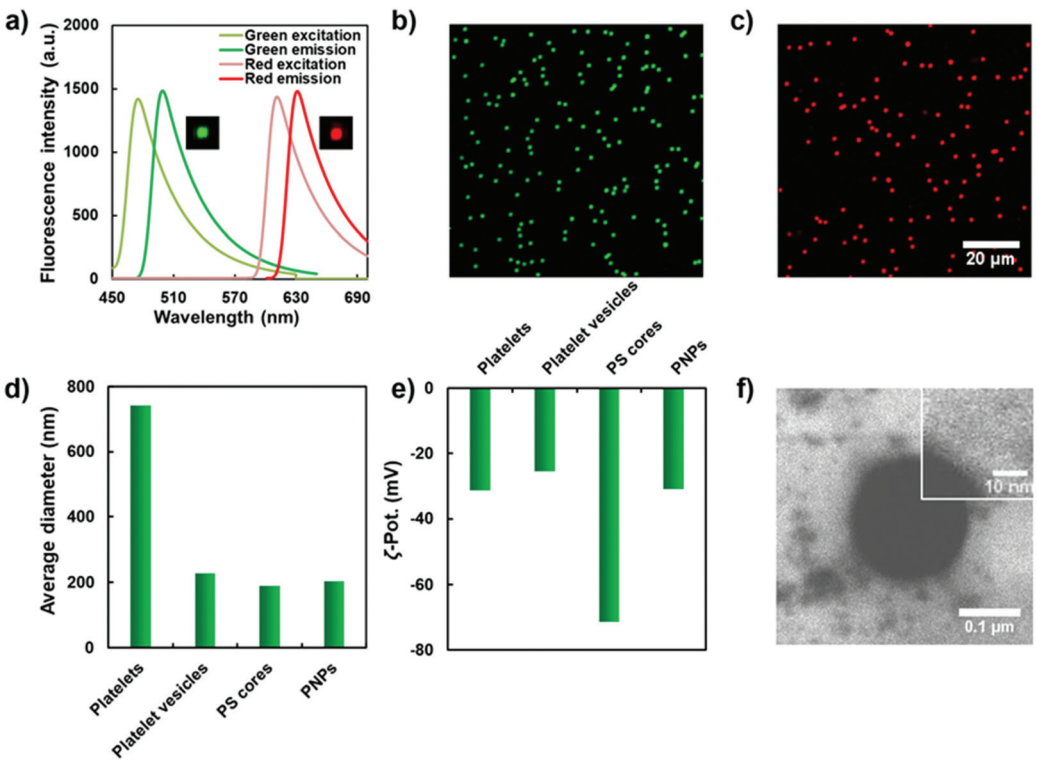

Fig. 1 (a) The excitation spectra and emission spectra of green and red fluorescent polystyrene nanoparticles (PS cores), respectively. (b) The fluorescence image of green PS cores. (c) The fluorescence image of red PS cores. (d) Average hydrodynamic size of platelets, platelet vesicles, PS cores and PNPs. (e) Zeta potential of platelets, platelet vesicles, PS cores and PNPs. (f) The TEM image of a single PNP.

Feasibility of fibrinogen detection using the SPD method

In order to verify the feasibility of fibrinogen detection, single-particle imaging experiments in the absence and presence of fibrinogen were performed on a LCSM. Firstly, green and red probes were mixed together in a 1 : 1 ratio. Without fibrinogen, there is almost no overlap between green and red fluorescence in the merged image (Fig. 2a, i–iii). However, in the presence of fibrinogen (300 μg mL^{-1}), the signal from the green and red channels are almost the same (Fig. 2b, i and ii). Meanwhile, yellow spots can be observed evidently in the merged channel (Fig. 2b, iii). In order to disclose the colocalization phenomenon in the merged channel more intuitively, a MATLAB program was used to extract the overlapped points in the merged image (see the ESI†). A noticeable difference was observed in the extraction results as shown in Fig. 2a, iv and b, iv. These results give clear evidence that the presence of fibrinogen induces the crosslinking of fluorescent probes and then results in the fluorescence colocalization between the green and red channels.

The scatter plot is one of the most commonly used methods for fluorescence colocalization analysis. Therefore, we acquired the RGB value of each pixel in the merged channel and drew scatter plots using the green and red components. In the absence of fibrinogen, the scatter plot tends to be divergent and most of the points accumulate on the axes (Fig. 2a, v), indicating that these two variables are randomly correlated under this condition. In contrast, in the presence of fibrinogen, the scatter plot shows a diagonal trend ($y = x$), which represents fairly strong positive correlation and a high degree of colocalization (Fig. 2b, v). Moreover, fluorescence colocalization can also be demonstrated by plotting the intensity profile from fluorescent spots in the region of interest, the results are shown in Fig. S4.† To further confirm that the fluorescence colocalization was caused by the formation of aggregated structures in the presence of target fibrinogen, the samples were imaged by using SEM. As shown in Fig. 2a, vi, the PNPs exhibit excellent monodispersity in the absence of fibrinogen. However, in the presence of fibrinogen, aggregated structures can be observed evidently in the SEM image (Fig. 2b, vi). Therefore, the above experimental results imply that the SPD method is feasible for sensitive fibrinogen analysis.

Quantitative detection of fibrinogen based on the SPD method

Prior to the SPD experiments, the optimal reaction time was investigated. In the experiments, 37 °C was used as the incubation temperature for the binding reaction, which does not destroy the conformation of fibrinogen and is suitable for the binding of fibrinogen and integrin receptors.[15] Fig. 3a shows the fluorescence imaging results under different incubation times (60, 90, 120 and 150 min). With the increment of time, the ratio of yellow fluorescence spots (representing the colocalization events) increases gradually. In our study, Pearson's

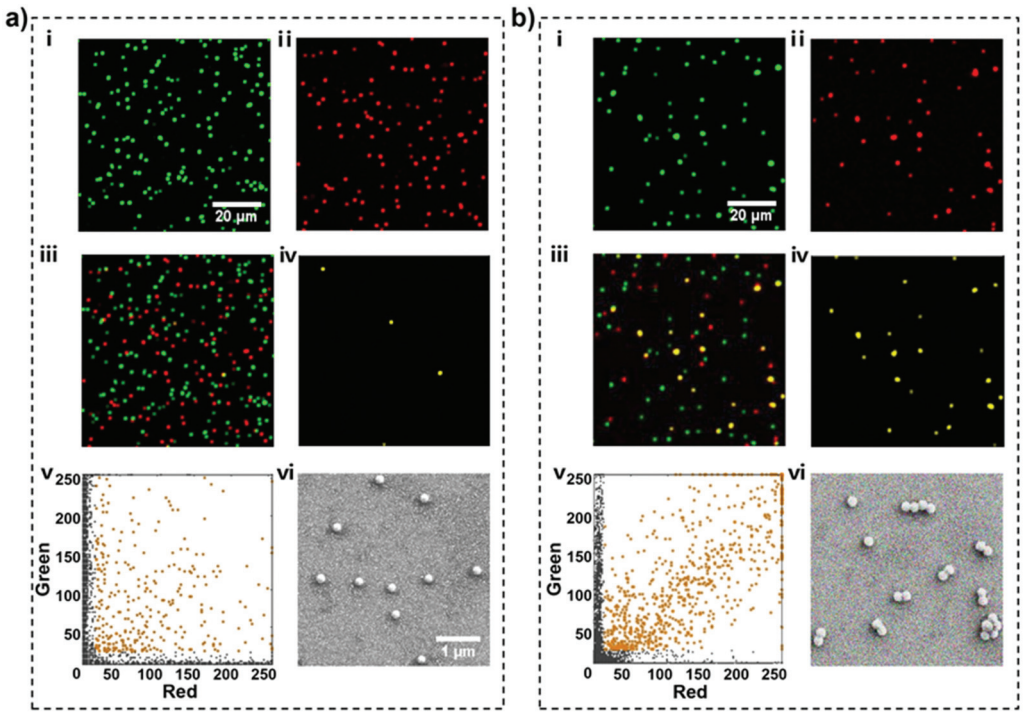

Fig. 2 (a) i. The green channel, ii. red channel, iii. merged channel of fluorescence images, iv. overlapped points, v. scatter plot (gray points represent background and un-correlated part; orange points represent correlated part) and vi. SEM image of green and red PNPs in the absence of fibrinogen. (b) i. The green channel, ii. red channel, iii. merged channel of fluorescence images, iv. overlapped points, v. scatter plot and vi. SEM image of green and red PNPs in the presence of 300 μg mL^{-1} fibrinogen.

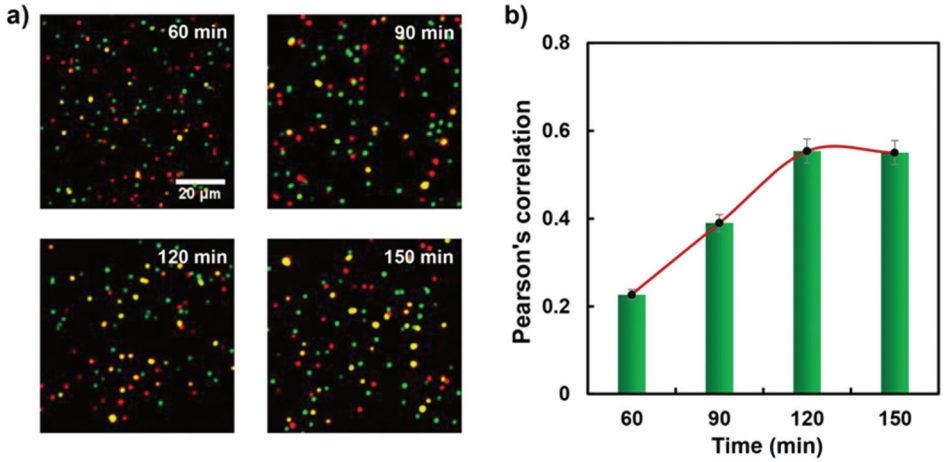

Fig. 3 Optimization of the experimental conditions for fibrinogen detection. (a) The fluorescence imaging results of 300 μg mL^{-1} fibrinogen detection under different incubation times (60, 90, 120 and 150 min). (b) The change of Pearson's correlation coefficient with incubation time.

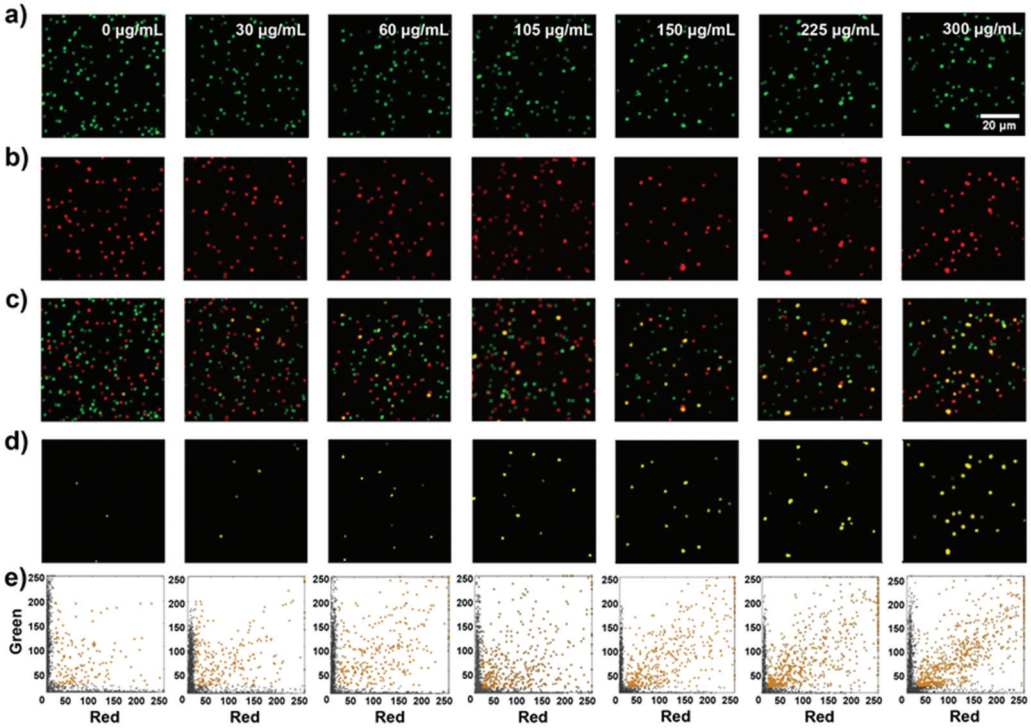

Fig. 4 (a) The green channel, (b) red channel, and (c) merged channel of fluorescence images, (d) overlapped points and (e) scatter plots (gray points represent background and un-correlated part; orange points represent correlated part) of green and red PNPs after being treated with different concentrations of fibrinogen (0, 30, 60, 105, 150, 225 and 300 μg mL^{-1}).

correlation coefficient was used as an index to quantify the degree of fluorescence colocalization (see the ESI†). As shown in Fig. 3b, the Pearson's correlation coefficient increases with time and reaches a plateau at about 120 min. Therefore, the optimal incubation time was set to be 120 min.

The sensitivity of the SPD method for fibrinogen quantification under the optimal conditions was investigated. In this experiment, PNPs were incubated with different concentration of fibrinogen solutions. Afterwards, the colocalization events of green and red fluorescence were observed using LCSM. As shown in Fig. 4a–e, the experimental results of green, red, and merged channels of fluorescence images, overlapped points and scatter plots were obtained under different fibrinogen concentrations (0, 30, 60, 105, 150, 225 and 300 μg mL^{-1}, from left to right). In the absence of fibrinogen, the fluorescence spots in the green and red channels are evenly distributed with

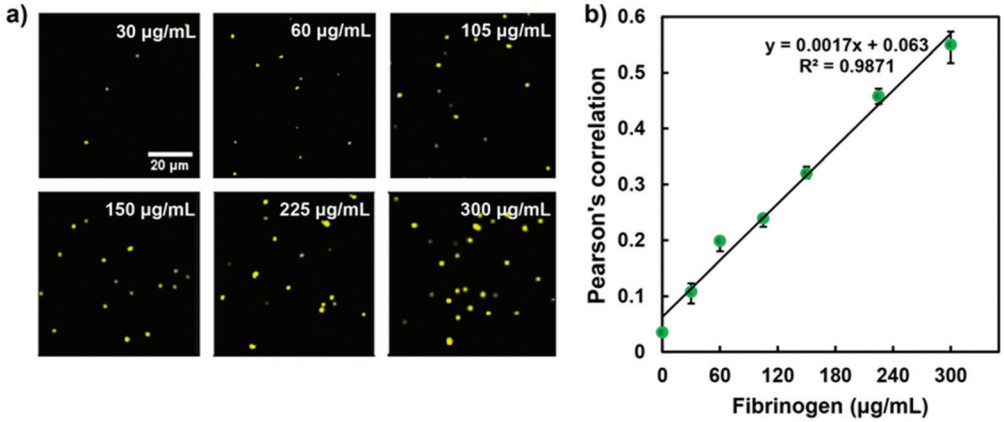

Fig. 5 The sensitivity of fibrinogen detection with PNPs. (a) The results of overlapped points under different fibrinogen concentrations. (b) The linear relationship between Pearson's correlation coefficient and fibrinogen concentration.

almost no overlap. With the increment of the fibrinogen concentration, more overlaps can be observed in the merged images (Fig. 4c). The number of overlapped points in Fig. 4d and variation trend of scatter plots in Fig. 4e also confirm this phenomenon.

Due to the binding of fibrinogen and PNPs, the Pearson's correlation coefficient which represents the colocalization events (Fig. 5a) increases from 0.028 to 0.552 as the concentration of fibrinogen increased from 0 to 300 μg mL^{-1}. As shown in Fig. 5b, the correlation coefficient manifests a good linear relationship (R^2 = 0.987, y = 0.0017x + 0.063) with fibrinogen concentrations in the range of 30–300 μg mL^{-1}. The LOD is 3.9 μg mL^{-1} (11.3 nM, evaluated from signal-to-noise ratio of 3) which is superior to most of the current methods (Table S1†).

Selectivity performance of the proposed fibrinogen detection method

To evaluate the selectivity of this method, various potential interfering substances were tested as controls. The non-target interfering substances detected in our study can be classified into three categories: (1) the corresponding ligands of the receptors on the platelet membrane: collagen and thrombin. (2) Common proteins that coexist with fibrinogen in plasma: BSA, TF and IgG. (3) Peptides and a variety of amino acids: GSH, L-Tyr, L-Phe, L-Lys and L-His, among which similar amino terminus may bind to fibrinogen. In the control experiments, the mixture of PNPs was incubated with the solutions containing fibrinogen (150 μg mL^{-1}, 0.435 μM), collagen (0.87 μM), thrombin (0.87 μM), BSA (0.87 μM), IgG (0.87 μM), TF (0.87 μM), GSH (0.87 μM) or amino acids (0.87 μM), respectively. Subsequently, the fluorescence images were acquired by LCSM. As shown in Fig. 6a, in the presence of fibrinogen, yellow fluorescence spots can be observed evidently. However, the colocalization events of non-target substances are insignificant compared with fibrinogen. Among the non-target interfering substances, collagen is the ligand of receptor $\alpha_2\beta_1$ on the platelet membrane. The receptor $\alpha_2\beta_1$ is poorly expressed on the platelet membrane compared with $\alpha_{IIb}\beta_3$. The experimental result showed that although the collagen concentration was two times higher than fibrinogen, the signal response was relatively weak (Pearson's correlation coefficient is 0.19). In

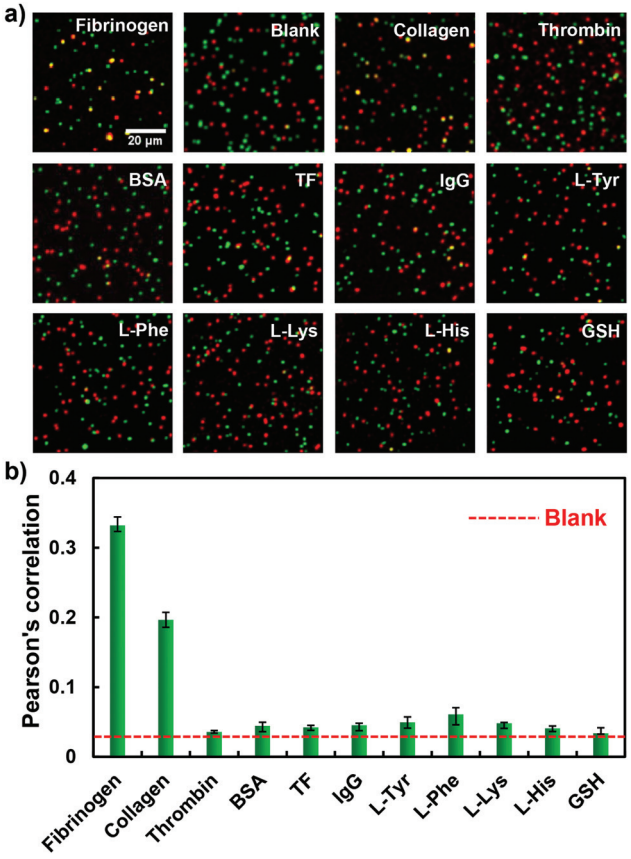

Fig. 6 The selectivity assay of fibrinogen detection. (a) The fluorescence images of green and red PNPs in the presence of 0.435 μM fibrinogen (150 μg mL^{-1}), 0 μM fibrinogen (blank) and 0.87 μM non-target compounds. (b) The corresponding Pearson's correlation coefficient of different samples in selectivity assay.

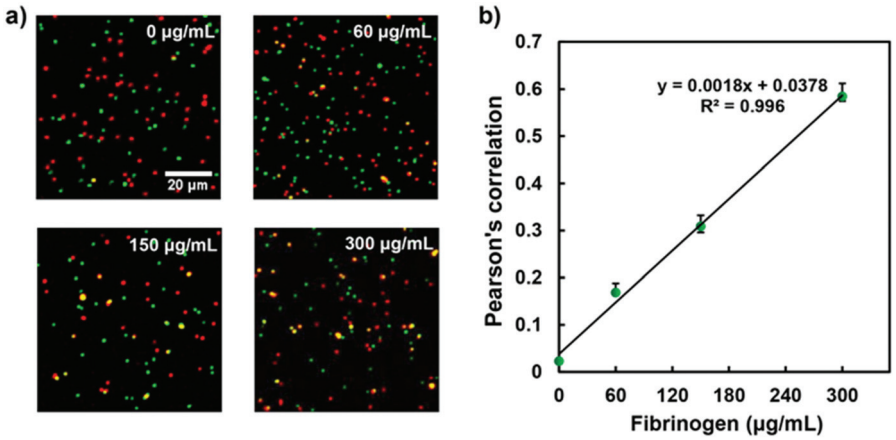

Fig. 7 Sensitive detection of fibrinogen in bovine plasma samples using PNPs. (a) The fluorescence images of PNPs in diluted-plasma samples spiked with different concentrations of fibrinogen (0, 60, 150 and 300 μg mL^{-1}). (b) The linear relationship between Pearson's correlation and fibrinogen concentration in real sample application.

addition, in the presence of other non-target substances, the colocalization event is almost negligible, which is the same as that obtained for the blank control. These results demonstrate that there is no significant specific interaction between the above interfering substances and PNPs compared with fibrinogen. This argument is confirmed by Pearson's correlation coefficients from these control groups (in the range of 0.03–0.07). In contrast, the signal response from the sample containing target fibrinogen was seven times higher (Pearson's correlation coefficient is 0.33), while the concentration of fibrinogen was even two times lower (Fig. 6b). Taken together, the developed SPD method in our study possesses excellent selectivity for fibrinogen detection.

Detection of fibrinogen in plasma samples

To investigate whether this method can detect fibrinogen in the bovine plasma sample, 1% PBS diluted plasma was spiked with different concentrations of fibrinogen (60, 150 and 300 μg mL^{-1}). As shown in Fig. 7a, without the addition of fibrinogen, there is almost no overlap between the fluorescence spots in the green and red channels. As the concentration of fibrinogen gradually increased, the fraction of colocalization events increases accordingly (Fig. 7a). As illustrated in Fig. 7b, the Pearson's correlation coefficient increases proportionally with fibrinogen concentrations (R^2 = 0.99, y = 0.0018x + 0.0378). Meanwhile, the spike recoveries and relative standard deviations (RSDs) (n = 3) were calculated to verify the reliability. As shown in Table 1, recoveries in the range of 98.3%–105.5% are obtained, indicating that the proposed method possesses reliable accuracy and promising capability for fibrinogen quantification in complex biological samples.

Table 1 Spike recovery of fibrinogen in 1% diluted plasma samples

Samples	Spiked fibrinogen (μg mL^{-1})	Measured (μg mL^{-1})	Recovery (%)	RSD (%)
1	60	63.3	105.5	7.1
2	150	147.4	98.3	5.3
3	300	312.6	104.2	4.7

Conclusion

In summary, we have developed a sensitive single-particle imaging method with PNPs for fibrinogen detection. Under optimal conditions, fibrinogen can be quantified in the range of 30–300 μg mL^{-1} with the LOD of 3.9 μg mL^{-1}. In addition, the selectivity of the biosensor is guaranteed by the specific binding between fibrinogen and PNPs. Upon application in real samples, it also showed good performance. This method overcomes the shortcoming of multi-factor dependence of traditional methods. It also avoids the antibody modification process in immunological methods which is complicated and expensive. The combination of SPD and cell membrane-coated nanotechnology brings additional advantages such as ultra-low sample consumption and excellent anti-interference ability. As a result, we believe that this new method will have great potential in fibrinogen quantification.

Author contributions

The manuscript was written through contributions of all authors. All authors have given approval to the final version of the manuscript.

Conflicts of interest

There are no conflicts to declare.

Acknowledgements

This work was supported by the National Natural Science Foundation of China (NSFC, Project No. 21974073).

References

1 L. Pous, S. S. Deshpande, S. Nath, S. Mezey, S. C. Malik, S. Schildge, C. Bohrer, K. Topp, D. Pfeifer, F. Fernandez-Klett, S. Doostkam, D. K. Galanakis, V. Taylor, K. Akassoglou and C. Schachtrup, *Nat. Commun.*, 2020, **11**, 630–642.
2 E. Y. L. Cheung, E. M. Weijers, B. Tuk, R. Scheffer, F. W. Leebeek, J. W. van Neck, P. Koolwijk and M. P. M. de Maat, *Tissue Eng., Part A*, 2015, **21**, 106–114.
3 J. J. Stec, H. Silbershatz, G. H. Tofler, T. H. Matheney and R. B. D'Agostino, *Circulation*, 2000, **102**, 1634–1638.
4 A. Zirlik, Y. Zhang, C. Zhu, Y. Guo, R. Xu, S. Li, Q. Dong and J. Li, *PLoS One*, 2014, **9**, 113460–113473.
5 K. E. McAleese, S. Graham, M. Dey, L. Walker, D. Erskine, M. Johnson, E. Johnston, A. J. Thomas, I. G. McKeith, C. DeCarli and J. Attems, *Brain Pathol.*, 2019, **29**, 414–424.
6 W. Gao, F. Zhang, T. Ma and J. Hao, *J. Gastric Cancer*, 2020, **20**, 202–211.
7 J. Yang, J. Ma, S. Cheng and Y. Wang, *OncoTargets Ther.*, 2020, **13**, 7283–7293.
8 S. Polterauer, V. Seebacher, K. Hefler-Frischmuth, C. Grimm, G. Heinze, C. Tempfer, A. Reinthaller and L. Hefler, *Am. J. Obstet. Gynecol.*, 2009, **200**, 641–647.
9 W. Miesbach, J. Schenk, S. Alesci and E. Lindhoff-Last, *Thromb. Res.*, 2010, **126**, e428–e433.
10 G. Piccione, S. Casella, C. Giannetto and E. Giudice, *J. Vet. Sci.*, 2010, **11**, 121–124.
11 S. Campuzano, V. Salema, M. Moreno-Guzman, M. Gamella, P. Yanez-Sedeno, L. A. Fernandez and J. M. Pingarron, *Biosens. Bioelectron.*, 2014, **52**, 255–260.
12 Z. L. Jiang, S. J. Sun, A. H. Liang and C. J. Liu, *Anal. Chim. Acta*, 2006, **571**, 200–205.
13 Z. Jiang, Y. Chen, A. Liang, H. Tao, N. Tang and F. Zhong, *Sci. China, Ser. B: Chem.*, 2007, **50**, 345–350.
14 S. Jo, I. Kim, W. Lee, M. Kim, J. Park, G. Lee, D. S. Yoon and J. Park, *Biosens. Bioelectron.*, 2019, **135**, 216–223.
15 J. Park, W. Lee, I. Kim, M. Kim, S. Jo, W. Kim, H. Park, G. Lee, W. Choi, D. S. Yoon and J. Park, *Sens. Actuators, B*, 2019, **293**, 296–303.
16 W. Chen, K. Zeng, H. Liu, J. Ouyang, L. Wang, Y. Liu, H. Wang, L. Deng and Y.-N. Liu, *Adv. Funct. Mater.*, 2017, **27**, 1605795–1605803.
17 Q. Hu, C. Qian, W. Sun, J. Wang, Z. Chen, H. N. Bomba, H. Xin, Q. Shen and Z. Gu, *Adv. Mater.*, 2016, **28**, 9573–9580.
18 T. Kang, Q. Zhu, D. Wei, J. Feng, J. Yao, T. Jiang, Q. Song, X. Wei, H. Chen, X. Gao and J. Chen, *ACS Nano*, 2017, **11**, 1397–1411.
19 J. D. Lapek Jr., R. H. Fang, X. Wei, P. Li, B. Wang, L. Zhang and D. J. Gonzalez, *ACS Nano*, 2017, **11**, 11831–11838.
20 K. Xiong, W. Wei, Y. Jin, S. Wang, D. Zhao, S. Wang, X. Gao, C. Qiao, H. Yue, G. Ma and H. Y. Xie, *Adv. Mater.*, 2016, **28**, 7929–7935.
21 L. Rao, L.-L. Bu, Q.-F. Meng, B. Cai, W.-W. Deng, A. Li, K. Li, S.-S. Guo, W.-F. Zhang, W. Liu, Z.-J. Sun and X.-Z. Zhao, *Adv. Funct. Mater.*, 2017, **27**, 1604774–1604783.
22 M. Xuan, J. Shao, L. Dai, J. Li and Q. He, *ACS Appl. Mater. Interfaces*, 2016, **8**, 9610–9618.
23 S. Thamphiwatana, P. Angsantikul, T. Escajadillo, Q. Zhang, J. Olson, B. T. Luk, S. Zhang, R. H. Fang, W. Gao, V. Nizet and L. Zhang, *Proc. Natl. Acad. Sci. U. S. A.*, 2017, **114**, 11488–11493.
24 R. H. Fang, A. V. Kroll, W. Gao and L. Zhang, *Adv. Mater.*, 2018, **30**, 1706759–1706792.
25 X. L. Lou, J. Sun, S. Q. Gong, X. F. Yu, R. Gong and H. Deng, *Chin. J. Cancer Res.*, 2015, **27**, 450–460.
26 L. Amo, E. Tamayo-Orbegozo, N. Maruri, C. Eguizabal, O. Zenarruzabeitia, M. Rinon, A. Arrieta, S. Santos, J. Monge, M. A. Vesga, F. Borrego and S. Larrucea, *Front. Oncol.*, 2014, **4**, 245–251.
27 F. A. Carvalho, S. Connell, G. Miltenberger-Miltenyi, S. V. Pereira, A. Tavares, R. A. S. Ariens and N. C. Santos, *ACS Nano*, 2010, **4**, 4609–4620.
28 C. M. Hu, R. H. Fang, K. C. Wang, B. T. Luk, S. Thamphiwatana, D. Dehaini, P. Nguyen, P. Angsantikul, C. H. Wen, A. V. Kroll, C. Carpenter, M. Ramesh, V. Qu, S. H. Patel, J. Zhu, W. Shi, F. M. Hofman, T. C. Chen, W. Gao, K. Zhang, S. Chien and L. Zhang, *Nature*, 2015, **526**, 118–121.
29 Q. Hu, W. Sun, C. Qian, C. Wang, H. N. Bomba and Z. Gu, *Adv. Mater.*, 2015, **27**, 7043–7050.
30 G. Tao, T. Lai, X. Xu, Y. Ma, X. Wu, X. Pei, F. Liu and N. Li, *Anal. Chem.*, 2020, **92**, 3697–3706.
31 Z. Ye, R. Weng, Y. Ma, F. Wang, H. Liu, L. Wei and L. Xiao, *Anal. Chem.*, 2018, **90**, 13044–13050.
32 Y. Han, Z. Ye, F. Wang, T. Chen, L. Wei, L. Chen and L. Xiao, *Nanoscale*, 2019, **11**, 14793–14801.
33 F. Wang, Y. Li, Y. Han, Z. Ye, L. Wei, H. B. Luo and L. Xiao, *Anal. Chem.*, 2019, **91**, 6329–6339.
34 Y. Han, Z. Ye, L. Chen and L. Xiao, *Anal. Chim. Acta*, 2020, **1109**, 53–60.
35 F. Wang, Y. Han, S. Wang, Z. Ye, L. Wei and L. Xiao, *Anal. Chem.*, 2019, **91**, 11856–11863.
36 F. Qi, Y. Han, H. Liu, H. Meng, Z. Li and L. Xiao, *Sens. Actuators, B*, 2020, **320**, 128347–128354.
37 X. Wei, J. Gao, R. H. Fang, B. T. Luk, A. V. Kroll, D. Dehaini, J. Zhou, H. W. Kim, W. Gao, W. Lu and L. Zhang, *Biomaterials*, 2016, **111**, 116–123.
38 D. Zhang, Z. Ye, L. Wei, H. Luo and L. Xiao, *ACS Appl. Mater. Interfaces*, 2019, **11**, 39594–39602.

